frontiers in Physics

ORIGINAL RESEARCH
published: 20 January 2021
doi: 10.3389/fphy.2020.593421

Epidemics Forecast From SIR-Modeling, Verification and Calculated Effects of Lockdown and Lifting of Interventions

R. Schlickeiser[1,2]* *and M. Kröger*[3]*

[1]*Institut für Theoretische Physik, Lehrstuhl IV: Weltraum- und Astrophysik, Ruhr-Universität Bochum, Bochum, Germany,* [2]*Institut für Theoretische Physik und Astrophysik, Christian-Albrechts-Universität zu Kiel, Kiel, Germany,* [3]*Polymer Physics, Department of Materials, ETH Zurich, Zurich, Switzerland*

Due to the current COVID-19 epidemic plague hitting the worldwide population it is of utmost medical, economical and societal interest to gain reliable predictions on the temporal evolution of the spreading of the infectious diseases in human populations. Of particular interest are the daily rates and cumulative number of new infections, as they are monitored in infected societies, and the influence of non-pharmaceutical interventions due to different lockdown measures as well as their subsequent lifting on these infections. Estimating quantitatively the influence of a later lifting of the interventions on the resulting increase in the case numbers is important to discriminate this increase from the onset of a second wave. The recently discovered new analytical solutions of Susceptible-Infectious-Recovered (SIR) model allow for such forecast. In particular, it is possible to test lockdown and lifting interventions because the new solutions hold for arbitrary time dependence of the infection rate. Here we present simple analytical approximations for the rate and cumulative number of new infections.

Keywords: coronavirus (2019-nCoV), statistical analysis, pandemic spreading, time-dependent infection rate, parameter estimation

OPEN ACCESS

Edited by:
Sen Pei,
Columbia University, United States

Reviewed by:
Ming Tang,
East China Normal University, China
Jiannan Wang,
Beihang University, China

***Correspondence:**
R. Schlickeiser
rsch@tp4.ruhr-uni-bochum.de
M. Kröger
mk@mat.ethz.ch

Specialty section:
This article was submitted to Social Physics, a section of the journal Frontiers in Physics

Received: *10 August 2020*
Accepted: *23 October 2020*
Published: *20 January 2021*

Citation:
Schlickeiser R and Kröger M (2021) Epidemics Forecast From SIR-Modeling, Verification and Calculated Effects of Lockdown and Lifting of Interventions. Front. Phys. 8:593421. doi: 10.3389/fphy.2020.593421

1 INTRODUCTION

The Susceptible-Infectious-Recovered (SIR) model has been developed nearly hundred years ago [1, 2] to understand the time evolution of infectious diseases in human populations. The SIR system is the simplest and most fundamental of the compartmental models and its variations [3–17]. The considered population of $N \gg 1$ persons is assigned to the three compartments s (susceptible), i (infectious), or r (recovered/removed). Persons from the population may progress with time between these compartments with given infection ($a(t)$) and recovery rates ($\mu(t)$) which in general vary with time due to non-pharmaceutical interventions taken during the pandemic evolution.

Let $I(t) = i(t)/N$, $S(t) = s(t)/N$ and $R(t) = r(t)/N$ denote the infected, susceptible and recovered/removed fractions of persons involved in the infection at time t, with the sum requirement $I(t) + S(t) + R(t) = 1$. In terms of the reduced time $\tau(t) = \int_0^t d\xi a(\xi)$, accounting for arbitrary but given time-dependent infection rates, the SIR-model equations are [1, 2, 18]

$$\frac{dI}{d\tau} = j - KI, \quad \frac{dS}{d\tau} = -j, \quad \frac{dR}{d\tau} = KI \tag{1}$$

in terms of the time-dependent ratio $K(t) = \mu(t)/a(t)$ of the recovery and infection rates and the medically interesting daily rate of new infections

$$\dot{J}(t) = a(t)j(\tau) = \dot{\tau}j(\tau), \tag{2}$$

where the dot denotes a derivative with respect to t.

For the special and important case of a time-independent ratio $K(t) = k = \text{const.}$ new analytical results of the SIR-model (1) have been recently derived [19] – hereafter referred to as paper A. The constant k is referred to as the inverse basic reproduction number $k = 1/R_0$. The new analytical solutions assume that the SIR equations are valid for all times $t \in [-\infty, \infty]$, and that time $t = \tau = 0$ refers to the "observing time" when the existence of a pandemic wave in the society is realized and the monitoring of newly infected persons $\dot{J}(t)$ is started. In paper A it has been shown that, for arbitrary but given infection rates $a(t)$, apart from the peak reduced time τ_0 of the rate of new infections, all properties of the pandemic wave as functions of the reduced time are solely controlled by the inverse basic reproduction number k. The dimensionless peak time τ_0 is controlled by k and the value $\varepsilon = -\ln S(0)$, indicating as only initial condition at the observing time the fraction of initially susceptible persons $S(0) = e^{-\varepsilon}$. This suggests to introduce the relative reduced time $\Delta = \tau - \tau_0$ with respect to the reduced peak time. In real time t the adopted infection rate $a(t)$ acts as second parameter, and the peak time t_m, where $\dot{J}(t)$ reaches its maximum must not coincide with the time, where the reduced j reaches its maximum, i.e., $\tau_m \equiv \tau(t_m) \neq \tau_0$, in general.

2 RESULTS AND DISCUSSION

According to paper A the three fractions of the SIR-model

$$\begin{aligned} &S(\tau) = 1 - J(\tau), \qquad I(\tau) = \frac{j(\tau)}{1 - J(\tau)}, \\ &R(\tau) = -k\ln[1 - J(\tau)] \end{aligned} \tag{3}$$

can be expressed in terms of the cumulative number $J(\tau)$ and differential daily rate $j(\tau) = dJ/d\tau$ of new infections. The cumulative number satisfies the nonlinear differential equation

$$j(\tau) = \frac{dJ}{d\tau} = (1 - J)[J + k\ln(1 - J)] \tag{4}$$

Two important values are $J_0(k) = J(\tau_0)$, where j attains its maximum with $(dj/dJ)_{J_0} = 0$, and the final cumulative number $J_\infty(k)$ at $\tau = t = \infty$, when the second bracket on the right-hand side of the differential **Eq. 4** vanishes, i.e., $J_\infty + k\ln(1 - J_\infty) = 0$. The two transcendental equations can be solved analytically in terms of Lambert's W function, as shown in paper A. In the present manuscript we are going to avoid Lambert's function completely, and instead use the following approximants (**Figure 1A**)

$$J_0(k) = (3 - k)(1 - k)\left(1 + k + k^2\right)/6, \tag{5}$$

$$J_\infty(k) = 1 - \exp[-(1 - k)(1 + \kappa)/k], \tag{6}$$

$$\kappa(k) = (4 - k)k/3 \tag{7}$$

Without any detailed solution of the SIR-model equations the formal structure of **Eqs 3** and **4** then provides the final values $I_\infty = j_\infty = 0$, $R_\infty = J_\infty$, and $S_\infty = 1 - J_\infty$. We list these values together with κ in **Table 1**. We emphasize that the final cumulative number J_∞, determined solely by the value of k, remains unchanged (**Table 1**). With NPIs one can only flatten and distort the epidemics curve (compared to the case of no NPIs taken) but not change the final cumulative number.

2.1 New infections

The exact solution of the differential **Eq. 4** is given in inverse form by (**Appendix A**)

$$\tau = \int_{1-e^{-\varepsilon}}^{J} \frac{dy}{(1 - y)[y + k\ln(1 - y)]}, \tag{8}$$

which can be integrated numerically (subject to numerical precision issues), replaced by the approximant presented in paper A (involving Lambert's function), or semi-quantitatively captured by the simple approximant to be presented next. The solution $J(\Delta)$ as a function of the relative reduced time $\Delta = \tau - \tau_0$, with the reduced peak time approximated by

$$\tau_0 = \frac{1 - k}{f_m(k)}\left[\ln\frac{J_0}{1 - J_0} - \ln\left(e^{\varepsilon} - 1\right)\right], \tag{9}$$

corresponding to $J = J_0$ in **Eq. 8**, and where $f_m(k) = 1 - k + \ln k$, is reasonably well captured by (**Appendix C**)

$$\begin{aligned} J(\Delta) = \frac{1}{2}[1 + \tanh Y_1(\Delta)]\Theta[\Delta_s(k) - \Delta] + \left\{1 - \frac{1 - J_\infty}{2}[1\right. \\ \left. + \coth Y_2(\Delta)]\right\}\Theta[\Delta - \Delta_s(k)] \end{aligned} \tag{10}$$

with the Heaviside step function $\Theta(x) = 1(0)$ for $x \geq (<)0$. In **Eq. 10**

$$\begin{aligned} Y_1 &= \frac{1}{2}\left[\frac{f_m(k)(\Delta - \Delta_s)}{1 - k} + \ln\frac{1 - k}{k}\right], \\ Y_2 &= \frac{1}{2}\left[E_0(k)(\Delta - \Delta_s) + \ln\frac{k}{(1 - k)\kappa}\right], \end{aligned} \tag{11}$$

with

$$\Delta_s = \frac{1 - k}{f_m(k)}\ln\frac{(1 - k)(1 - J_0)}{kJ_0}, \qquad E_0(k) = \left[\frac{k}{(1 - k)\kappa} - 1\right]f_m(k) \tag{12}$$

also tabulated in **Table 1**. We note that $\Delta_s(k)$ is always positive. **Figure 2** shows the approximation (**Eq. 10**) for the cumulative number as a function of the relative reduced time Δ for different values of k. For a comparison with the exact variation obtained by the numerical integration of **Eq. 8** see **Appendix C**. The agreement is remarkably well with maximum deviations less than 30 percent. The known limiting case of $k = 0$ is captured exactly by the approximant (**Appendix D**).

For the corresponding reduced differential rate $j(\Delta)$ in reduced time we use the right hand side of **Eq. 4** with $J = J(\Delta)$ from **Eq. 10**, cf. **Figure 3**. Note, that this j is not

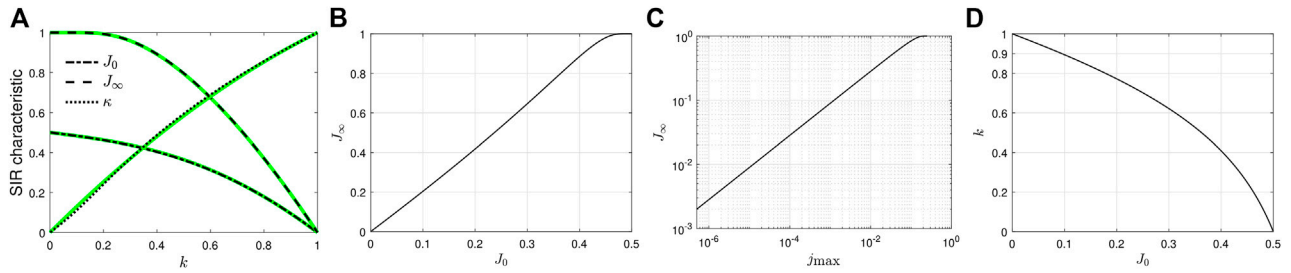

FIGURE 1 | (A) Approximants J_0, J_∞, and κ (thick green) used in this manuscript, cf. **Eqs (5)–(7)**, compared with the exact functions [19] (thin black). **(B)** J_∞ vs. J_0 and **(C)** J_∞ vs. $j_{\max}$ for the SIR model. **(D)** k as function of J_0 according to **Eq. 14**. For $J_0 \leq 0.1$ this is well approximated by $k \approx 1 - J_0$, where J_0 can be replaced by the cumulative fraction of infected people at the time of the maximum in the daily number of newly infected people.

TABLE 1 | Exact parameter values depending on the inverse basic reproduction number k.

k	κ	J_0	J_∞	S_∞	f_m	E_0	Δ_s	$j_{\max}$
0.00	0.00	0.500	1.000	0.000	1.000	0.0000	∞	0.2500
0.05	0.05	0.492	1.000	0.000	0.800	0.0000	3.5339	0.2327
0.10	0.11	0.483	1.000	0.000	0.670	0.0003	3.0441	0.2156
0.15	0.17	0.473	0.999	0.001	0.565	0.0049	2.7698	0.1986
0.20	0.24	0.462	0.993	0.007	0.478	0.0173	2.5745	0.1819
0.25	0.31	0.450	0.980	0.020	0.403	0.0348	2.4181	0.1653
0.30	0.37	0.436	0.959	0.041	0.339	0.0535	2.2835	0.1490
0.35	0.43	0.421	0.930	0.070	0.283	0.0709	2.1621	0.1330
0.40	0.49	0.403	0.893	0.107	0.234	0.0857	2.0491	0.1174
0.45	0.54	0.384	0.848	0.152	0.191	0.0971	1.9418	0.1022
0.50	0.59	0.363	0.796	0.203	0.153	0.1050	1.8386	0.0876
0.55	0.64	0.339	0.739	0.261	0.121	0.1093	1.7386	0.0736
0.60	0.69	0.313	0.676	0.324	0.094	0.1099	1.6416	0.0603
0.65	0.73	0.283	0.607	0.393	0.070	0.1071	1.5477	0.0479
0.70	0.78	0.251	0.533	0.467	0.050	0.1009	1.4571	0.0365
0.75	0.82	0.217	0.454	0.546	0.034	0.0914	1.3701	0.0263
0.80	0.86	0.179	0.371	0.629	0.022	0.0788	1.2871	0.0174
0.85	0.89	0.138	0.284	0.716	0.012	0.0633	1.2084	0.0102
0.90	0.93	0.095	0.193	0.807	0.005	0.0449	1.1343	0.0047
0.95	0.97	0.049	0.098	0.902	0.001	0.0237	1.0648	0.0012
1.00	1.00	0.000	0.000	1.000	0.000	0.0000	1.0000	0.0000

identical with the one obtained via $j = dJ/d\tau$, because J does not solve the SIR equations exactly. The peak value $j_{\max}$ in the reduced time rate occurs when $J = J_0$ and is thus determined by $j_{\max} = (1 - J_0)(1 - J_0 - k)$, also tabulated in **Table 1**.

As can be seen in **Figure 3** the rate of new infections (**Eq. 12**) is strictly monoexponentially increasing $j(\Delta \ll 0) \simeq e^{\Gamma_1 \Delta}$ with $\Gamma_1(k) = f_m(k)/(1-k)$ well before the peak time, and strictly monoexponentially decreasing well above the peak time $j(\Delta \gg 0) \propto e^{-\Gamma_2 \Delta}$ with the $\Gamma_2 = (1 - J_\infty)\Gamma_1/\kappa$. These exponential rates exhibit a noteworthy property and correlation in reduced time:

$$\frac{\Gamma_2}{\Gamma_1} = \frac{1 - J_\infty}{\kappa} \tag{13}$$

The SIR parameter k affects several key properties of the differential and cumulative fractions of infected persons. If the maximum $\dot{J}(t_m)$ of the measured daily number of newly infected persons has passed already, we find it most convenient to estimate k from the cumulative value $J(t_m)$ at this time t_m. While the maximum of $\dot{J}(t)$ must not occur exactly at $\tau(t_m) = \tau_0$ (**Appendix F**), we can still use J_0 as an approximant for the value of $J(t_m)$ and the relationship between J_0 and k can be inverted to read (**Appendix E**)

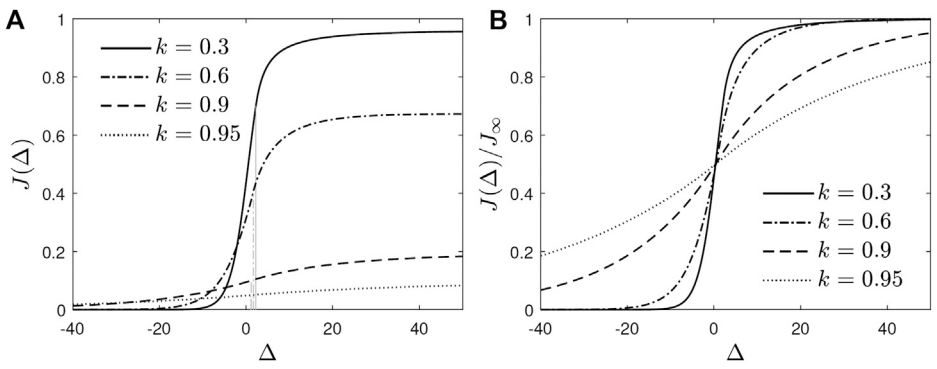

FIGURE 2 | (A) Cumulative number $J(\Delta)$ for different values of k according to **Eq. 10**. The vertical gray lines starting at the Δ-axis indicate the respective values of $\Delta_s(k)$. **(B)** Same as in **(A)**, divided by the final J_∞.

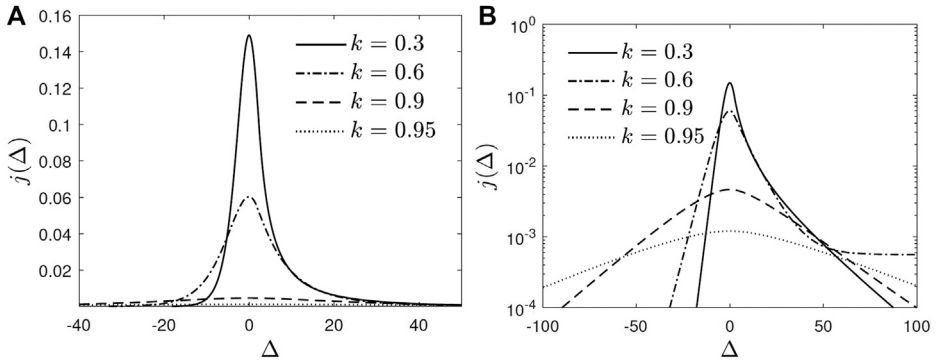

FIGURE 3 | Reduced differential rate $j(\Delta)$ of newly infected fraction corresponding to the cumulative $J(\Delta)$ shown in **Figure 2**. **(A)** linear scale, **(B)** semilogarithmic scale.

$$k = \frac{2(1-J_0)-1}{1+\ln(1-J_0)} = 1 - J_0 - \frac{J_0^2}{2} + O(J_0^3) \tag{14}$$

The dependency of k on J_0 is shown in **Figure 1C**. With the so-obtained value for k at hand, the infection rate $a(t_m)$ at peak time can be inferred from $a(t_m) = \dot{J}(t_m)/j_{\max}(k)$. It provides a lower bound for a_0.

A major advantage of the new analytical solutions in paper A and here is their generality in allowing for arbitrary time-dependencies of the infection rate $a(t)$. Such time-dependencies result at times greater than the observing time $t = 0$ from non-pharmaceutical interventions (NPIs) taken after the pandemic outbreak [20] such as case isolation in home, voluntary home quarantine, social distancing, closure of schools and universities and travel restrictions including closure of country borders, applied in different combinations and rigor [21] in many countries. These NPIs lead to a significant reduction of the initial constant infection rate a_0 at later times. It is also important to estimate the influence of a later lifting of the NPIs on the resulting increase in the case numbers in order to discriminate this increase from the onset of a second wave. Especially in the papers by Dehning et al. [17], Flaxman et al. [22] and those reviewed by Estrada [4] the influence of NPIs on the time evolution of the Covid-19 pandemics has been studied using numerical solutions of the SIR-model equations. Our analytical study presented here is superior to these results from numerical simulations as its predictions are particularly robust for the late forecast of the pandemic wave.

2.2 Modeling in Real Time of Lockdowns

The corresponding daily rate $\dot{J}(t)$ and cumulative number $J(t)$ of new infections in real time t for given time-dependent infection rates $a(t)$ are $J(t) = J(\tau(t))$ and $\dot{J}(t)$ given by **Eq. 2**. From a medical point of view the daily rate $\dot{J}(t)$ is most important as it determines also i) the fatality rate [23] $d(t) \simeq f\dot{J}(t - t_d)$ with the fatality percentage $f \simeq 0.005$ in countries with optimal medical services and hospital capacities and the delay time of $t_d \simeq 7$ days, ii) the daily number of new seriously sick persons [24] NSSPs = $2f\dot{J}(t - t_d)$ needing access to breathing apparati, and iii) the day of maximum rush to hospitals $t_r = t_m + t_d$. In countries with poor medical and hospital capacities and/or limited access to them the fatality percentage is significantly higher by a factor h which can be as large as 10.

To calculate the rate and cumulative number in real time according to **Eq. 2** we adopt as time-dependent infection rate the integrable function known from shock wave physics

$$a_{\rm LD}(t) = \frac{a_0}{2}\left[1 + q - (1-q)\tanh\frac{t-t_a}{t_b}\right] \simeq \begin{cases} a_0 & \text{for } t \ll t_a \\ qa_0 & \text{for } t \gg t_a, \end{cases} \tag{15}$$

which implies

$$\begin{aligned} \tau_{\rm LD}(t) &= \frac{a_0}{2}\left[(1+q)t - (1-q)t_b \ln\left(\frac{\cosh\frac{t-t_a}{t_b}}{\cosh\frac{t_a}{t_b}}\right)\right] \\ &\simeq \begin{cases} a_0 t & \text{for } t \ll t_a \\ qa_0 t & \text{for } t \gg t_a \end{cases} \end{aligned} \tag{16}$$

The time-dependent lockdown infection rate (**Eq. 15**) is characterized by four parameters: i) the initial constant infection rate a_0 at early times $t \ll t_a$, ii) the final constant infection rate $a_1 = qa_0$ at late times $t \gg t_a$ described by the quarantine factor $q = a_1/a_0 \le 1$, first introduced in Refs. 21 and 24, iii) the time t_a of maximum change, and iv) the time t_b regularizing the sharpness of the transition. The latter is known to be about $t_b \simeq 7$–14 days reflecting the typical 1–2 weeks incubation delay. Consequently, the parameter q mainly affects the amplitude $\dot{J}$ shown in the left columns of **Figures 5** and **6** (note that we also plotted the case of no NPIs taken (i.e., $q = 1$) for comparison). Alternatively, the transition time t_b controls the rapidness of the transition in the fraction of infected persons per day and therefore the widespread.

Moreover, the initial constant infection rate a_0 characterizes the Covid-19 virus: if we adopt the German values $a_0 \simeq 58\ \text{days}^{-1}$ and $t_b \simeq 11$ determined below, with the remaining two parameters q and t_a we can represent with the chosen functional form **Eq. 15** four basic types of reductions: 1) drastic (small $q \ll 1$) and rapid (t_a small), 2) drastic (small $q \ll 1$) and late (t_a large), 3) mild (greater q) and rapid (t_a small), and 4) mild (greater q) and late (t_a large). The four types are exemplified in **Figure 4**.

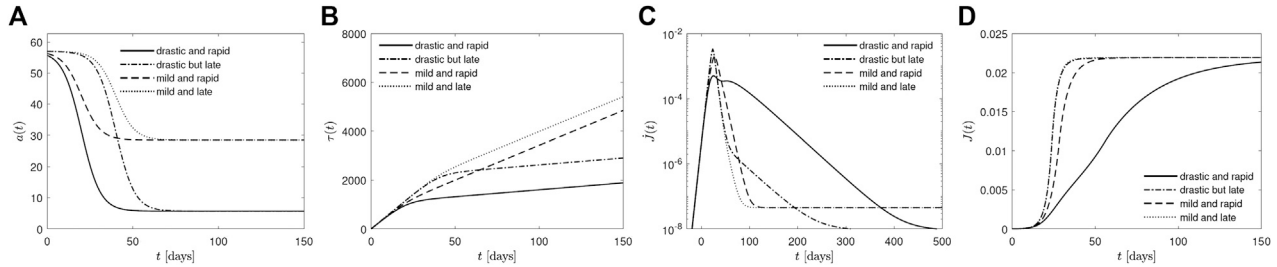

FIGURE 4 | (A) Infection rate $a(t)$, **(B)** reduced time $\tau(t)$, **(C)** daily rate of new infections $\dot{J}(t)$, **(D)** cumulative fraction $J(t)$ of infected persons. In each panel we consider four basic types of reductions: 1) drastic (small $q = 0.1$) and rapid ($t_a = 20$), 2) drastic (small $q = 0.1$) and late ($t_a = 40$), 3) mild ($q = 0.5$) and rapid ($t_a = 20$), and 4) mild ($q = 0.5$) and late ($t_a = 40$). Remaining parameters due to Germany: $t_b = 11$ days, $a_0 = 57$ days^{-1}, and $k = 0.989$. Both curves in **(C)** for the late cases reach the same value at the maximum, which is plausible as the curve remains unaffected at the time of the maximum. The rapid cases tend to lower the maximum amplitude already at the time of the maximum, and thus tend to decrease it compared with the late cases.

2.3 Verification and Forecast

In countries where the peak of the first Covid-19 wave has already passed such as e.g. Germany, Switzerland, Austria, Spain, France and Italy, we may use the monitored fatality rates and peak times to check on the validity of the SIR model with the determined free parameters. However, later monitored data are influenced by a time varying infection rate $a(t)$ resulting from non-pharmaceutical interventions (NPIs) taken during the pandemic evolution. Only at the beginning of the pandemic wave it is justified to adopt a time-independent injection rate $a(t) \simeq a_0$ implying $\tau = a_0 t$. Alternatively, also useful for other countries which still face the climax of the pandemic wave, it is possible to determine the free parameters from the monitored cases in the early phase of the pandemic wave. We illustrate our parameter estimation using the monitored data from Germany with a total population of 83 million persons ($P = 8.3 \times 10^7$).

In Germany the first two deaths were reported on March 9 so that $\varepsilon = 4.8 \times 10^{-6}$ corresponding to about 400 infected people 7 days earlier, on March 2 ($t = 0$). The maximum rate of newly infected fraction, $\dot{J}_{\max} \simeq 380/fP$, occurred $t_m = 37$ days later, consistent with a peak time of fatalities on 16 April 2020. At peak time the cumulative death number was $D_m = 3820/P$ corresponding to $J_m = D_m/f = 200 D_m = 0.009$. This implies $k \approx 1 - J_0 \approx 0.991$ according to **Eq. 14** (and not far from the value $k = 0.989$ to be determined from the fit shown in **Figure 5**). From the initial exponential increase of daily fatalities in Germany we extract $\Gamma_1(k) a_0 \simeq 0.28$, corresponding to a doubling time of $\ln(2)/\Gamma_1 a_0 \simeq 2.3$ days, as we know $\Gamma_1(k) = f_m(k)/(1-k) \simeq 0.0046$ already from the above k. The quantity a_m we can estimate from the measured $\dot{J}_{\max}$, as $\dot{J}_{\max} = a_m j_{\max}$ and $j_{\max}(k) \approx 4.2 \times 10^{-5}$. Using the mentioned value for $\dot{J}_{\max}$, we obtain $a_m \approx 22$/days as a lower bound for a_0.

With these parameter values the entire following temporal evolution of the pandemic wave in Germany can be predicted as function of t_b and q. To obtain all parameters consistently, we fitted the available data to our model without constraining any of the parameters (**Figure 5**). This yields for Germany $k \simeq 0.989$, $t_a \simeq 21$ days, $q \simeq 0.15$, $a_0 \simeq 58$ days, and $t_b = 11$ days. The obtained parameters allow us to calculate the dimensionless peak time $\tau_m \simeq 1353$, the dimensionless time $\tau_0 \simeq 1390$, as well as $J_m \simeq 0.009$, $J_0 \simeq 0.011$, $\Gamma_1 \simeq 0.0056$ and $\Gamma_2 \simeq 0.0055$.

We note that the value of $k = 0.989$ implies for Germany that $J_\infty(0.989) = 0.022$ according to **Figure 1**, so that at the end of the first Covid-19 wave in Germany 2.2% of the population, i.e., 1.83 million persons will be infected. This number corresponds to a final fatality number of $D_\infty = 9146$ persons in Germany.

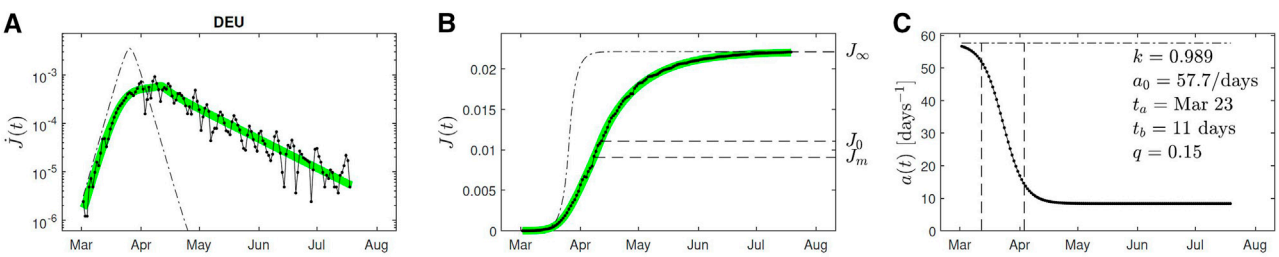

FIGURE 5 | (A) Measured data $\dot{J}(t)$ of new daily infected fraction (black circles) for Germany (DEU) compared with the model $\dot{J}(t) = a(t) j(\tau(t))$ outlined here (green). Shown for comparison is the case where no NPIs are imposed ($q = 1$, black dot-dashed). **(B)** The measured cumulative fraction $J(t)$ (black circles) together with the model prediction (green), and the reference $q = 1$ case. Also depicted are J_0 and the value at peak time, J_m. **(C)** The infection rate $a(t)$ corresponding to the curves shown in **(A)** and **(B)**. Model parameters mentioned in the figure; a dropped from an initial value of $\simeq 58$/days down to 7.8/days during the 2nd half of march. This realized case can be directly compared with the four hypothetic cases shown in **Figure 4**. For details on how to obtain the parameters see **Appendix G**.

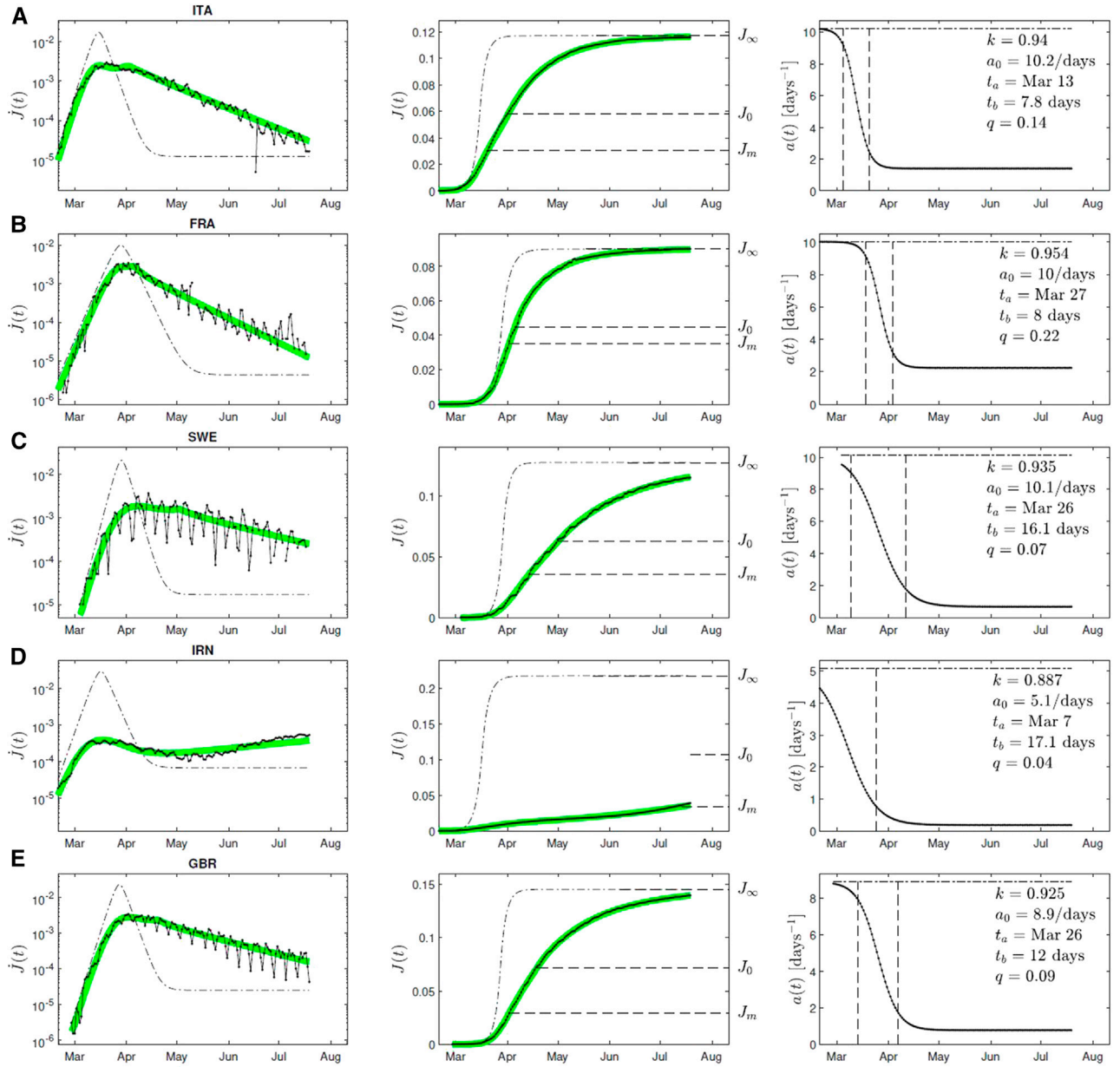

FIGURE 6 | Same as **Figure 5** for other countries: **(A)** Italy (ITA), **(B)** France (FRA), **(C)** Sweden (SWE), **(D)** Iran (IRN), **(E)** Great Britain (GBR).

Of course, these numbers are only valid estimates if no efficient vaccination against Covid-19 will be available.

An important consequence of the small quarantine factor $q = 0.15$ is the implied flat exponential decay after the peak. Because $\Gamma_1 \simeq \Gamma_2$ for $k = 0.989$, the exponential decay is by a factor q smaller than the exponential rise prior the climax, i.e.,

$$\dot{J}(t \gg t_m) \propto e^{-\Gamma_2 a_0 q t} = e^{-\frac{\Gamma_1 (1-J_\infty) a_0 q t}{\kappa}} \simeq e^{-t/21.8 \text{ days}} \tag{17}$$

Equation 17 yields a decay half-live of $\ln(2) \times 21.8$ days $\simeq 15$ days to be compared with the initial doubling time of $\simeq 2.3$ days. For Germany we thus know that their lockdown was drastic and rapid: the time $t_a \simeq$ March 23 is early compared to the peak time $t_m \simeq$ April 8 resulting in a significant decrease of the infection rate with the quarantine factor $q \simeq a_m/a_0 = 0.15$. In **Figure 5** we calculate the resulting daily new infection rate as a function of the time t for the parameters for Germany, and compare with the measured data. In the meantime, the strict lockdown interventions have been lifted in Germany: this does not effect the total numbers J_∞ and D_∞ but it should reduce the half-live decay time further.

We also performed this parameter estimation for other countries with sufficient data. For some of them data is visualized in **Figure 6**, parameters for the remaining countries are tabulated in **Tables 2** and **3**. Most importantly, with the

TABLE 2 | Model parameters and model implications. The columns are as follows: country (α_3 code), population P in millions (M), outbreak time defining $t = 0$, fitted time t_a, estimated time t_0 corresponding to the reduced peak time τ_0 of $j(\tau)$, fitted SIR parameter k, fitted initial infection rate a_0, fitted parameter t_b, fitted quarantine factor q, estimated doubling time t_2 characterizing the early exponential increase, estimated decay half life t_2' characterizing the late exponential decrease, estimated unreported number of infections per reported number, estimated final fraction J_∞ of infected population, final number of estimated fatalities $D_\infty P = J_\infty P f$. We use $f = 0.005$ as the probability to decease from a Covid-19 infection (reported plus unreported).

country	P/M	$t = 0$	t_a	t_m	t_0	k	a_0	t_b	q	t_2	t_2'	dark	J_∞	$D_\infty P$
AFG	34.66	Mar 18	Apr 3	Jul 7	Jun 28	0.995	68.9	36	0.16	4.0	24.8	7.1	1.00%	1725
ALB	2.88	Mar 11	Mar 22	Jul 17	Jul 19	0.988	24.4	1	0.14	4.7	34.2	6.8	2.41%	346
AND	0.08	Mar 19	Mar 25	Mar 23	Apr 4	0.931	7.6	0	0.24	2.6	12.0	11.8	13.50%	52
ARG	43.85	Mar 6	Apr 4	Jul 13	Jul 19	0.987	21.8	12	0.20	4.8	24.1	4.6	2.63%	5774
ARM	2.93	Mar 22	Jun 9	Jul 1	Jul 19	0.897	1.1	14	0.30	11.4	43.7	4.0	19.78%	2893
AUT	8.75	Mar 9	Mar 11	Mar 31	Apr 5	0.992	149.8	19	0.05	1.1	23.4	7.2	1.66%	725
BEL	11.35	Mar 4	Mar 28	Apr 3	Apr 9	0.911	6.1	7	0.23	2.5	12.3	30.8	17.30%	9822
BFA	18.65	Mar 14	Mar 20	Mar 19	Apr 5	0.999	1754.5	0	0.25	2.8	10.9	10.1	0.06%	53
BGR	7.13	Mar 7	Mar 31	Jul 15	Jul 19	0.974	10.1	28	0.12	5.3	47.3	7.8	5.10%	1828
BLR	9.51	Mar 25	Mar 19	Jun 25	Jul 19	0.975	40.9	32	0.03	1.4	55.1	1.6	4.91%	2344
BOL	10.89	Mar 23	Apr 12	Jun 24	Jul 3	0.968	7.9	29	0.31	5.5	18.4	8.7	6.30%	3428
BRA	207.65	Mar 11	Mar 15	May 27	Jul 13	0.919	12.1	46	0.02	1.4	64.9	8.3	15.83%	164365
CAF	4.60	May 24	May 27	Jun 15	Jun 14	0.999	123.9	11	1.87	9.3	5.0	2.6	0.24%	55
CHE	8.37	Mar 1	Mar 22	Mar 23	Apr 3	0.976	22.0	5	0.25	2.6	10.9	11.8	4.70%	1969
CHL	17.91	Mar 16	Jun 7	Jul 9	Jul 8	0.910	2.0	11	0.22	7.5	38.3	5.5	17.43%	15610
CHN	1378.67	Jan 15	Feb 1	Apr 9	Feb 16	0.999	1544.6	9	0.09	2.6	28.1	10.9	0.07%	4765
COL	48.65	Mar 15	Apr 4	Jul 16	Jul 19	0.899	4.0	7	0.19	3.3	20.1	8.4	19.48%	47385
CUB	11.48	Mar 19	Mar 22	Apr 16	Apr 15	0.999	631.5	21	0.25	2.9	11.5	7.1	0.15%	86
CZE	10.56	Mar 17	Mar 25	Apr 1	Apr 11	0.997	235.1	8	0.08	1.7	21.4	5.3	0.69%	365
DEU	82.67	Mar 2	Mar 23	Apr 8	Apr 11	0.989	57.7	11	0.15	2.2	15.1	9.0	2.21%	9146
DNK	5.73	Mar 8	Mar 23	Mar 28	Apr 8	0.989	52.6	6	0.16	2.4	15.3	9.2	2.15%	615
DOM	10.65	Mar 12	Mar 23	Jul 17	Jul 19	0.747	2.6	16	0.04	1.9	76.4	4.0	45.91%	24442
DZA	40.61	Mar 6	Mar 31	Apr 2	Jul 19	0.977	18.4	9	0.05	3.3	65.2	10.0	4.48%	9105
ECU	16.39	Mar 7	Mar 7	Apr 25	Jul 8	0.935	15.5	40	0.01	1.3	119.5	14.9	12.72%	10422
EGY	95.69	Mar 6	Apr 3	Jun 8	Jun 22	0.994	52.5	5	0.22	4.4	19.8	10.5	1.20%	5724
ESP	46.44	Feb 26	Mar 17	Mar 25	Mar 31	0.937	12.4	6	0.14	1.7	13.4	21.9	12.27%	28498
ETH	102.40	Mar 29	Mar 29	Jul 19	Jul 10	0.999	215	4	1.29	21	16.2	4.7	0.06%	315
FRA	66.90	Feb 19	Mar 27	Apr 2	Apr 5	0.954	10.0	8	0.22	3.0	14.2	28.5	9.01%	30142

exception of the six countries ARM, DOM, IRN, PAN, PER, SMR we found values of $k > 0.9$ for all other countries investigated corresponding to basic reproduction numbers $R_0 = 1/k < 1.11$. These values are significantly smaller than the estimates of $R_0 \in [2.4, 5.6]$ in the mainstream literature on Covid-19 [4, 22]. Part of these significant differences may be explained by the different definitions of R_0.

While the inverse basic reproduction number $k = 1/R_0 = \mu(t)/a(t)$ in the SIR-model is clearly defined as the ratio of the recovery to infection rate, there are alternative definitions of the basic reproduction number R_0 using the effective reproduction factor $R(t)$. As discussed in detail in Sect. 4 of Ref. 25 $R(t)$ has to be calculated from the convolution

$$R(t) = \frac{c(t)}{\int_0^\infty ds\, W(s) c(t-s)} \tag{18}$$

of the number of daily cases $c(t)$ with the serial interval distribution $W(t)$ describing the probability for the time lag between a person's infection and the subsequent transmission of the virus to a second person. As different choices of the serial interval distribution are used in the literature this leads to differences in the calculated associated effective reproduction factors $R(t)$. As R_0 is identical to the value $R(t_0)$ at the starting time of the outbreak it is not clear in the moment that this R_0 will be identical to the $1/k$ of the SIR model [26].

2.4 Summary and Conclusion

In this work we derived for the first time an analytical approximation for the solution for the SIR-model equations with an accuracy better than 30 percent. The explicit approximation refers to the fraction of newly infected persons per day $\dot{J}$ as a function of the relative reduced time with respect to the reduced peak time. This closed form of the analytical solution only depends on a single parameter k, the ratio of infection to recovery rates. We assume that this ratio is independent of time. As $\dot{J}$ can be directly compared with the monitored death and infection rates in different countries, we see no advantage in using the more complicated SEIR-model which currently does not allow for a closed analytical solution. An analytic solution of the SIR model with an accuracy better than 5% is available as well from our yet unpublished work where we did not consider time-dependent $a(t)$, but it has the disadvantage that it involves Lambert's function.

For the first time in the history of SIR-research (these equations have been discovered 93 years ago!) we thus have derived an analytical solution which can be applied successfully to all accumulated data of virus diseases in the world. Being of analytic form it is superior to all existing numerical simulations and results in the literature. We also discovered for the first time how to extract the value of k from the monitored data which is highly nontrivial. We applied this new method to the data taken

TABLE 3 | Continuation of **Table 2**.

country	P/M	$t = 0$	t_a	t_m	t_0	k	a_0	t_b	q	t_2	t_2'	dark	J_∞	$D_\infty P$
GAB	1.98	Apr 16	Apr 30	Jun 8	Jun 6	0.997	64.6	0	0.39	7.6	19.4	1.6	0.56%	56
GBR	65.64	Feb 29	Mar 26	Apr 2	Apr 19	0.925	8.9	12	0.09	2.0	26.1	30.9	14.54%	47719
GHA	28.21	Mar 16	Mar 21	Jun 12	Jun 18	0.999	464.9	0	0.22	4.4	19.9	1.2	0.13%	190
GRC	10.75	Mar 7	Mar 24	Mar 27	Apr 7	0.998	191.9	6	0.16	3.8	24.6	10.1	0.38%	203
GTM	16.58	Mar 28	Jun 11	Jul 7	Jul 6	0.985	9.7	10	0.48	9.4	19.9	9.0	3.03%	2513
HND	9.11	Mar 22	Mar 28	Jun 24	Jul 14	0.978	26.0	17	0.11	2.5	23.5	6.6	4.28%	1952
HRV	4.17	Mar 19	Apr 11	Apr 11	Apr 28	0.996	72.3	17	0.04	4.8	122.5	6.3	0.79%	165
IND	1324.17	Mar 6	Mar 21	Jun 8	Jun 28	0.997	189.9	36	0.12	2.4	20.8	5.9	0.61%	40316
IRL	4.77	Mar 7	Mar 13	Apr 17	Apr 16	0.962	21.2	29	0.11	1.7	16.9	13.7	7.41%	1768
IRN	80.28	Feb 12	Mar 8	Jul 14	Jul 19	0.819	3.1	17	0.04	2.3	84.0	11.5	33.82%	135755
ITA	60.60	Feb 15	Mar 13	Mar 20	Apr 1	0.940	10.2	8	0.14	2.2	17.6	28.7	11.70%	35442
KOR	25.37	Feb 14	Feb 16	Mar 14	Mar 21	0.999	989.6	13	0.07	1.2	17.4	4.3	0.22%	285
KWT	4.05	Apr 6	May 5	May 22	Jun 6	0.986	21.8	20	0.09	4.5	51.0	1.5	2.83%	573
LBN	6.01	Mar 4	Mar 31	Jul 19	Jul 19	0.999	95.5	2	0.09	9.9	105.3	3.6	0.29%	88
LUX	0.58	Mar 11	Mar 19	Apr 4	Apr 4	0.981	29.5	7	0.21	2.4	12.1	4.0	3.82%	111
MAR	35.28	Mar 10	Mar 24	Mar 28	Apr 17	0.999	628.8	13	0.03	2.5	82.8	3.6	0.18%	316
MDA	3.55	Mar 20	Mar 25	Jun 1	Jun 15	0.973	25.9	23	0.06	1.9	33.7	7.0	5.40%	960
MEX	127.54	Mar 13	Mar 24	Jul 19	Jun 24	0.954	16.2	42	0.06	1.8	31.1	25.4	8.99%	57326
MKD	2.08	Mar 16	Mar 31	Jun 25	Jul 19	0.927	5.4	9	0.11	3.4	33.1	10.1	14.29%	1488
MRT	4.30	May 6	Jun 1	Jun 3	Jun 7	0.996	66.4	4	0.29	5.1	17.9	5.3	0.82%	175
MYS	31.19	Mar 10	Mar 17	Mar 15	Mar 30	0.999	2064.2	7	0.11	1.7	16.2	2.8	0.08%	123
NGA	185.99	Mar 23	Apr 25	Jun 9	Jun 24	0.999	405.4	21	0.16	5.2	33.1	4.7	0.13%	1214
NLD	17.02	Mar 1	Mar 22	Mar 31	Apr 8	0.963	15.4	5	0.20	2.4	12.6	23.7	7.26%	6182
NPL	28.98	May 10	Jun 2	May 29	Jun 20	0.999	953.4	3	0.34	7.7	22.5	0.5	0.04%	55
PAK	193.20	Mar 11	Apr 8	Jun 11	Jun 13	0.997	101.1	17	0.22	4.0	18.2	4.4	0.69%	6677
PAN	4.03	Mar 15	Mar 26	Jul 10	Jul 19	0.848	3.5	10	0.09	2.5	35.5	4.8	28.80%	5808
PER	31.78	Mar 13	Mar 6	Jul 16	Jul 19	0.703	3.2	47	0.03	1.3	68.9	10.1	52.66%	83666
PHL	103.32	Mar 5	Mar 23	Jul 5	Jul 19	0.996	142.4	19	0.04	2.5	58.0	5.7	0.78%	4024
POL	37.95	Mar 6	Apr 2	Apr 17	Jun 5	0.993	63.1	20	0.05	3.4	67.0	8.3	1.30%	2474
PRT	10.33	Mar 11	Mar 14	Mar 31	Apr 22	0.982	86.4	16	0.02	0.9	38.8	7.1	3.67%	1896
ROU	19.71	Mar 15	Mar 17	Jul 14	Jul 19	0.909	13.8	21	0.02	1.1	79.1	11.7	17.60%	17343
RUS	144.34	Mar 18	Mar 18	May 22	Jul 5	0.984	60.7	44	0.02	1.4	61.8	3.4	3.12%	22543
SEN	15.41	Mar 28	May 9	Jun 8	Jun 24	0.998	79.9	1	0.55	11.5	21.0	4.3	0.30%	232
SMR	0.03	Mar 3	Mar 13	Mar 13	Mar 19	0.867	2.9	0	0.41	3.5	10.4	12.0	25.32%	42
SOM	15.01	Apr 6	Apr 19	Apr 15	May 4	0.999	591.7	0	0.24	3.7	15.2	6.0	0.13%	95
SRB	7.06	Mar 15	Mar 25	Jul 19	Jul 19	0.931	10.1	15	0.03	1.9	73.7	5.1	13.50%	4763
SWE	9.90	Mar 7	Mar 26	Apr 14	May 1	0.935	10.1	16	0.07	2.1	33.6	14.7	12.75%	6311
TCD	15.48	Apr 21	Apr 28	Apr 30	May 4	0.999	1387.0	3	0.22	2.1	9.2	16.9	0.10%	75
THA	68.86	Mar 17	Mar 29	Mar 26	Apr 1	0.999	3463.0	0	0.56	4.8	8.6	3.6	0.02%	58
TUN	11.40	Mar 15	Mar 30	Mar 26	Apr 1	0.999	659.7	6	0.29	4.7	16.4	7.3	0.09%	50
TUR	79.51	Mar 12	Mar 17	Apr 9	May 6	0.990	144	21	0.01	1.0	108.3	5.1	1.97%	7851
USA	323.13	Feb 24	Mar 23	Apr 10	May 16	0.938	10.2	23	0.03	2.1	81.6	7.8	12.18%	196763
ZAF	55.91	Mar 22	May 18	Jul 14	Jul 19	0.968	6.5	21	0.32	6.6	21.1	3.7	6.34%	17728

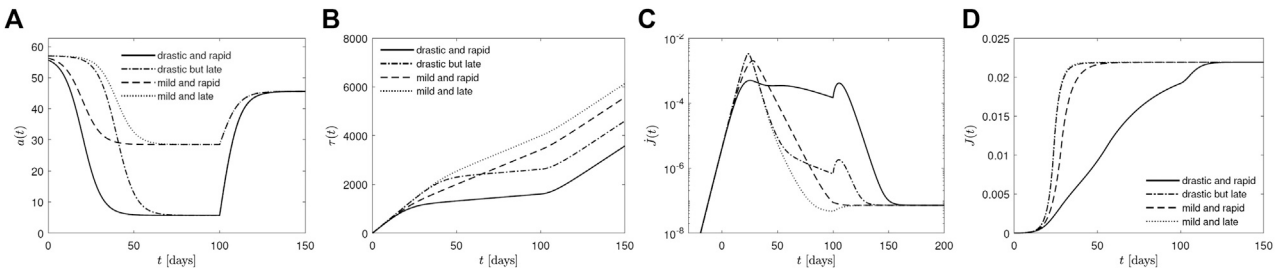

FIGURE 7 | Same as **Figure 4** but with incomplete lifting ($\eta = 0.8$) hundred days after breakout ($t_s = 100$ days). **(A)** infection rate $a(t)$, **(B)** reduced time $\tau(t)$, **(C)** daily rate of new infections $\dot{J}(t)$, **(D)** cumulative fraction $J(t)$ of infected persons. In each panel we consider four basic types of reductions: 1) drastic (small $q = 0.1$) and rapid ($t_a = 20$), 2) drastic (small $q = 0.1$) and late ($t_a = 40$), 3) mild ($q = 0.5$) and rapid ($t_a = 20$), and 4) mild ($q = 0.5$) and late ($t_a = 40$). Remaining parameters due to Germany: $t_b = 11$ days, $a_0 = 57$ days^{-1}, and $k = 0.989$.

for the Covid-19 pandemic waves in many countries. Our work includes an estimate on the effects of non-pharmaceutical interventions in these countries. This is possible as our analytical solution holds for arbitrary but given time dependencies $a(t)$ of the infection rates.

An example, on how lockdown lifting can be modeled is described in **Appendix H**. The situation is depicted in **Figure 7**. The lifting will increase $a(t)$ from its present value up to a value that might be close to the initial a_0. While the dynamics is altered, the final values remain unaffected by the dynamics, except, if the first pandemic wave is followed by a 2nd one. The values for J_∞ provided in **Tables 2** and **3** provide a hint on how likely is a 2nd wave. These values correspond to the population fraction that had been infected already. While this fraction is extremely large in Peru (53%), it is still below 1% in several of the larger countries. The tables also report the unreported number of infections per reported number (column "dark"), estimated from the number of fatalities, reported infections, and the death probability f.

DATA AVAILABILITY STATEMENT

Publicly available datasets were analyzed in this study. This data can be found here: https://pomber.github.io/covid19/timeseries.json.

AUTHOR CONTRIBUTIONS

All authors listed have made a substantial, direct, and intellectual contribution to the work and approved it for publication.

REFERENCES

1. Kermack WO, McKendrick AG. A contribution to the mathematical theory of epidemics. *Proc R Soc A* (1927) 115:700–21.
2. Kendall DG. Deterministic and stochastic epidemics in closed populations. In: Conference third Berkeley symposium on mathematical statistics and probability; 1955 Jul–Aug. Vol. 4. Berkeley, CA: University of California Press (1956) p. 149–65.
3. Hethcode HW. The mathematics of infectious diseases. *SIAM Rev* (2000) 42: 599–653. doi:10.1137/s0036144500371907
4. Estrada E. Covid-19 and sars-cov-2. modeling the present, looking at the future. *Phys Rep* (2020) 869:1–51. doi:10.1016/j.physrep.2020.07.005
5. O'Regan SM, Kelly TC, Korobeinikov A, O'Callaghan MJA, Pokrovskii AV. Lyapunov functions for SIR and SIRS epidemic models. *Appl Math Lett* (2010) 23:446–8. doi:10.1016/j.aml.2009.11.014
6. Satsuma J, Willox R, Ramani A, Grammaticos B, Carstea AS. Extending the SIR epidemic model. *Phys Stat Mech Appl* (2004) 336:369–75. doi:10.1016/j.physa.2003.12.035
7. Cadoni M. How to reduce epidemic peaks keeping under control the time-span of the epidemic. *Chaos Solitons Fractals* (2020) 138:109940. doi:10.1016/j.chaos.2020.109940
8. Cadoni M, Gaeta G. Size and timescale of epidemics in the sir framework. *Phys D* (2020) 411:132626. doi:10.1016/j.physd.2020.132626
9. Chekroun A, Kuniya T. Global threshold dynamics of an infection age-structured SIR epidemic model with diffusion under the Dirichlet boundary condition. *J Diff Equ* (2020) 269:117–48. doi:10.1016/j.jde.2020.04.046
10. Imron C, HariyantoYunus M, Surjanto SD, Dewi NAC. Stability and persistence analysis on the epidemic model multi-region multi-patches. *J Phys Conf Ser* (2019) 1218: 012035. doi:10.1088/1742-6596/1218/1/012035
11. Karaji PT, Nyamoradi N. Analysis of a fractional SIR model with general incidence function. *Appl Math Lett* (2020) 108:106499. doi:10.1016/j.aml.2020.106499
12. Mohamadou Y, Halidou A, Kapen PT. A review of mathematical modeling, artificial intelligence and datasets used in the study, prediction and management of Covid-19. *Appl Intell* (2020) 50, 3913–25. doi:10.1007/s10489-020-01770-9
13. Samanta S, Sahoo B, Das B. Dynamics of an epidemic system with prey herd behavior and alternative resource to predator. *J Phys Math Theor* (2019) 52: 425601. doi:10.1088/1751-8121/ab264d
14. Sene N. SIR epidemic model with mittag-leffler fractional derivative. *Chaos Solitons Fractals* (2020) 137:109833. doi:10.1016/j.chaos.2020.109833
15. Simon M. SIR epidemics with stochastic infectious periods. *Stoch Process their Appl* (2020) 130:4252–4274. doi:10.1016/j.spa.2019.12.003
16. Tian C, Zhang Q, Zhang L. Global stability in a networked SIR epidemic model. *Appl Math Lett* (2020) 107:106444. doi:10.1016/j.aml.2020.106444
17. Dehning J, Zierenberg J, Spitzner FP, Wibral M, Neto JP, Wilcek M, et al. Inferring change points in the spread of COVID-19 reveals the effectiveness of interventions. *Science* (2020) 369:eabb9789. doi:10.1126/science.abb9789
18. Barmparis GD, Tsironis GP. Estimating the infection horizon of covid-19 in eight countries with a data-driven approach. *Chaos Solitons Fractals* (2020) 135:109842. doi:10.1016/j.chaos.2020.109842
19. Kröger M, Schlickeiser R. Analytical solution of the SIR-model for the temporal evolution of epidemics. part a: time-independent reproduction factor. *J Phys A* (2020) 53:505601. doi:10.20944/preprints202007.0416.v1
20. Ferguson N, Laydon D, Nedjati-Gilani G. *Impact of non-pharmaceutical interventions (NPIs) to reduce COVID-19 mortality and healthcare demand*. London: Imperial College London (2020) doi:1025561/77482
21. Schlickeiser R, Kröger M. Dark numbers and herd immunity of the first covid-19 wave and future social interventions. *Epidem Int J* (2020) 4:000152. doi:10.23880/eij-16000152
22. Flaxman S, Mishra S, Mishra S, Gandy A, Unwin HJT, Mellan TA, et al. Estimating the effects of non-pharmaceutical interventions on Covid-19 in Europe. *Nature* (2020) 584:257–261. doi:10.1038/s41586-020-2405-7
23. Schüttler J, Schlickeiser R, Schlickeiser F, Kröger M. Covid-19 predictions using a gauss model, based on data from april 2. *Physics* (2020) 2:197–212. doi:10.3390/physics2020013
24. Schlickeiser R, Schlickeiser F. A Gaussian model for the time development of the sars-cov-2 corona pandemic disease. predictions for Germany made on 30 March 2020. *Physics* (2020) 2:164–70. doi:10.3390/physics2020010
25. Kröger M, Schlickeiser R. Gaussian doubling times and reproduction factors of the Covid-19 pandemic disease. *Front Phys* (2020) 8:276. doi:10.3389/fphy.2020.00276
26. Schlickeiser R, Kröger M. First consistent determination of the basic reproduction number for the first Covid-19 wave in 71 countries from the SIR-epidemics model with a constant ratio of recovery to infection rate. *Global J Front Res F* (2020) 20:37–43. doi:10.3929/ethz-b-000456421

Conflict of Interest: The authors declare that the research was conducted in the absence of any commercial or financial relationships that could be construed as a potential conflict of interest.

APPENDIX A: NON-PARAMETRIC SOLUTION OF THE SIR MODEL

We start from the Eq. 19 from part A

$$\tau = \int_{\varepsilon}^{G} \frac{dx}{1 - e^{-x} - kx} \tag{A1}$$

and substitute

$$y = 1 - e^{-x},\ x = -\ln(1-y),\ \frac{dx}{dy} = \frac{1}{1-y} \tag{A2}$$

Consequently, as the cumulative number of new infections is given (see Eq. 37 from part A) by

$$\tau = \int_{\psi}^{J} \frac{dy}{(1-y)f(y)},\quad f(y) = y + k\ln(1-y) \tag{A3}$$

with the abbreviation $\psi = J(0) = 1 - e^{-\varepsilon}$ for the initial value. This inverse relation $\tau(J)$ is the general solution of the SIR-model for constant k. It is not in parametrized form.

APPENDIX A.1: Maximum of *j*

Taking the derivative of Eq. 37 from part A with respect to τ we obtain

$$1 = \frac{j}{(1-J)[J + k\ln(1-J)]} \tag{A4}$$

or the exact SIR relation

$$j = (1-J)[J + k\ln(1-J)] \tag{A5}$$

Equation A5 provides

$$\frac{dj}{dJ} = 1 - k - 2J - k\ln(1-J) \tag{A6}$$

The maximum value $j_{\max}$ occurs for $(dj/dJ)_{J_0} = 0$ providing

$$1 - J_0 = \frac{k\ln(1-J_0) + k + 1}{2} \tag{A7}$$

Setting $1 - J_0 = e^{-X}$ yields

$$e^{-X} = -\frac{k}{2}\left(X - \frac{k+1}{k}\right), \tag{A8}$$

which is of the form of Eq. G1 from part A, and solved in terms of the non-principal Lambert function W_{-1} as

$$X = \frac{k+1}{k} + W_{-1}(\alpha_0),\quad \alpha_0 = -\frac{2}{ke}e^{-1/k,} \tag{A9}$$

so that

$$J_0 = 1 - e^{-\frac{1+k}{k} - W_{-1}(\alpha_0)} = 1 + \frac{k}{2}W_{-1}(\alpha_0) \tag{A10}$$

The maximum value is then given by

$$j_{\max} = j(J_0) = \frac{k^2}{4}\{[1 + W_{-1}(\alpha_0)]^2 - 1\} \tag{A11}$$

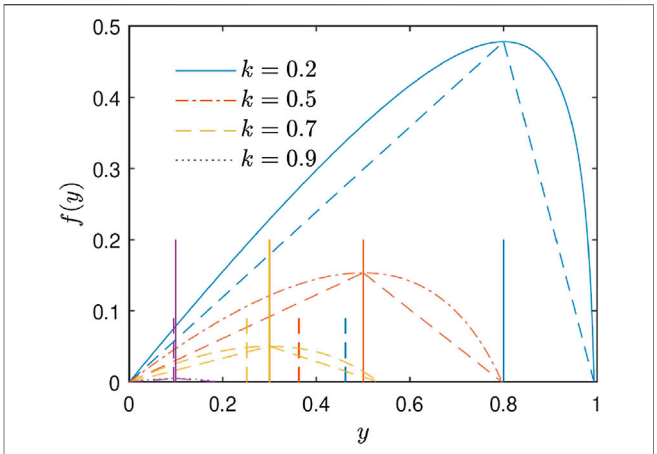

FIGURE B1 | Comparison of the approximation (B2) with the exact curve for $f(y)$ for different values of k. Vertical solid lines mark the position of the maximum of the function.

and this can also be written as $j_{\max} = (1-J_0)(1-J_0-k)$ with J_0 from **Eq. A10**. According to **Eq. 8** the reduced peak time in the dimensionless rate of new infections is then given by

$$\tau_0 = \int_{\psi}^{J_0} \frac{dy}{(1-y)f(y)}, \tag{A12}$$

which is the only quantity depending besides on k also on ε via $\psi = 1 - e^{-\varepsilon}$. In order to have our approximation depending only on k we therefore introduce the relative reduced time with respect to the peak reduced time

$$\Delta = \tau - \tau_0 = \int_{J_0}^{J} \frac{dy}{(1-y)f(y)} \tag{A13}$$

which is still exact, independent of ε and only determined by the value of k.

APPENDIX B: APPROXIMATING THE FUNCTION *f* (y)

The function $f(y)$ defined in **Eq. A3** vanishes for $y_c + k\ln(1-y_c) = 0$, or $1 - y_c = e^{-y_c/k}$ with the solution

$$y_c(k) = J_\infty(k) = (1-k)(1+\kappa) \tag{B1}$$

where κ was already stated in the introduction. According to **Eq. A13** the value J_∞ corresponds to $\Delta = \tau = \infty$, so the maximum value of the cumulative number of new infections is $J_{\max} = J_\infty$.

Moreover, the function $f(y)$ attains its maximum value $f_m(k) = f(y = 1-k) = 1 - k + k\ln k$ at $y_m = 1 - k$. As approximation we use

$$f(y) \simeq \begin{cases} f_1(y) & \text{for } y \le 1-k \\ f_2(y) & \text{for } (1-k) \le y \le J_\infty \end{cases} = f_m \begin{cases} \dfrac{y}{1-k} & \text{for } y \le 1-k \\ \dfrac{J_\infty - y}{J_\infty - (1-k)} & \text{for } 1-k \le y \le J_\infty \end{cases} \tag{B2}$$

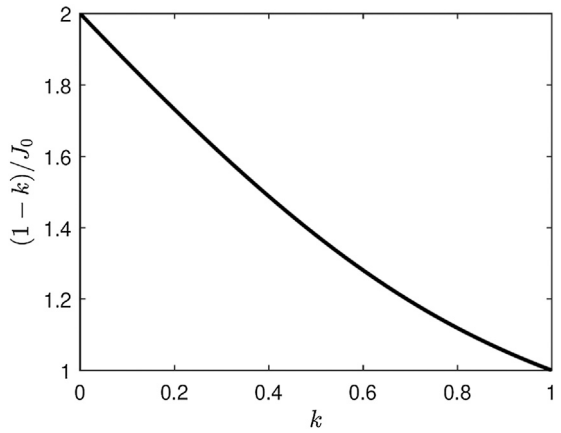

FIGURE C1 | The ratio $(1-k)/J_0(k)$ as a function of k.

which is shown in **Figure B1** in comparison with the function $f(y)$. The agreement is reasonably well with maximum deviations less than 30%.

APPENDIX C: APPROXIMATIONS FOR $J(\tau)$

Figure C1 demonstrates that $J_0(k)$ is always smaller than $1-k$. In order to calculate the integral in **Eq. A13** with the approximation **Eq. B1** we then have to investigate two cases: 1) For $J_0 < 1-k$ and $J < 1-k$ only the function f_1 contributes and

$$\Delta_{(J<1-k,J_0<1-k)} = \int_{J_0}^{J} \frac{dy}{(1-y)f_1(y)} \tag{C1}$$

2) For $J \geq 1-k > J_0$ both functions f_1 and f_2 contribute and

$$\begin{aligned}\Delta_{(J\geq 1-k>J_0)} &\simeq \int_{J_0}^{1-k} \frac{dy}{(1-y)f_1(y)} + \int_{1-k}^{J} \frac{dy}{(1-y)f_2(y)} \\ &= \Delta_s + \int_{1-k}^{J} \frac{dy}{(1-y)f_2(y)}\end{aligned} \tag{C2}$$

with

$$\begin{aligned}\Delta_s &= \int_{J_0}^{1-k} \frac{dy}{(1-y)f_1(y)} = \frac{1-k}{f_m(k)}\int_{J_0}^{1-k} \frac{dy}{(1-y)y} = \frac{1-k}{f_m(k)}\ln\frac{\frac{1}{J_0}-1}{\frac{1}{1-k}-1} \\ &= \frac{1-k}{f_m(k)}\ln\frac{(1-J_0)(1-k)}{kJ_0}\end{aligned} \tag{C3}$$

denoting the relative time corresponding to the value $J = 1-k$. We consider each case in turn.

Appendix C.1 Case (1): $J \leq 1-k$, $J_0 < 1-k$

Here **Eq. C1** provides

$$\frac{f_m\Delta}{1-k} = \int_{J_0}^{J} \frac{dy}{(1-y)y} = \ln\frac{\frac{1}{J_0}-1}{\frac{1}{J}-1}, \tag{C4}$$

so that the difference of **Eqs C3** and **C4** yields

$$\frac{f_m(\Delta-\Delta_s)}{1-k} = \ln\frac{kJ}{(1-k)(1-J)}, \tag{C5}$$

or after inversion

$$J(\tau) = \left[1 + \frac{k}{1-k}e^{-\frac{f_m(\Delta-\Delta_s)}{1-k}}\right]^{-1} \tag{C6}$$

Appendix C.2 Case (2): $J \geq 1-k > J_0$

Here **Eq. C2** with **Eq. C3** yields

$$\begin{aligned}f_m\Delta &\simeq (1-k)\int_{J_0}^{1-k} \frac{dy}{(1-y)y} + [J_\infty - (1-k)]\int_{1-k}^{J} \frac{dy}{(1-y)(J_\infty - y)} \\ &= f_m\Delta_s + (J_\infty - 1 + k)\int_{1-k}^{J} \frac{dy}{(1-y)(J_\infty - y)},\end{aligned} \tag{C7}$$

so that

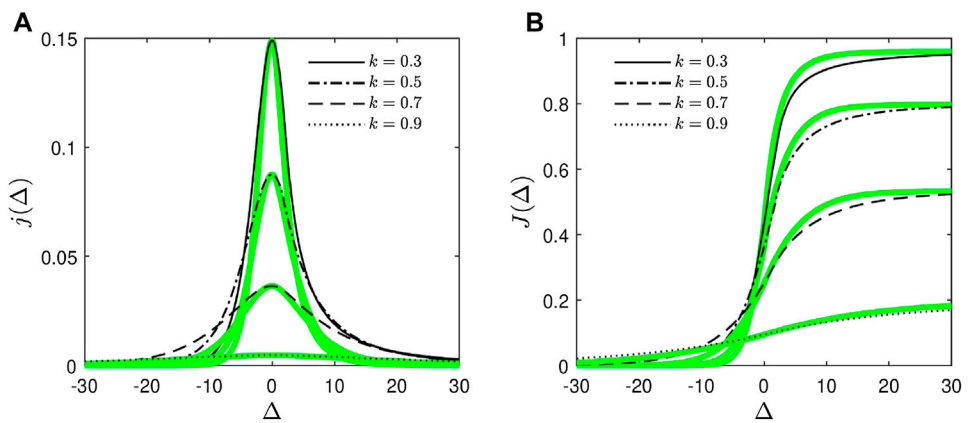

FIGURE C2 | Comparison for **(A)** $j(\Delta)$ and **(B)** $J(\Delta)$ between exact solution of the SIR model (green) and the approximant used here (black) for various k. Our approximant [19] in terms of Lambert's function is shown as well, but coincides with the exact solution (green) in this representation.

$$\frac{f_m(\Delta-\Delta_s)}{J_\infty-(1-k)}=\int_{1-k}^{J}\frac{dy}{(1-y)(J_\infty-y)}=-\frac{1}{1-J_\infty}\ln\frac{1-\frac{1-J_\infty}{1-J}}{1-\frac{1-J_\infty}{k}}$$
$$=-\frac{1}{1-J_\infty}\ln\frac{k(J_\infty-J)}{(J_\infty-1+k)(1-J)} \tag{C8}$$

After straightforward but tedious algebra we obtain

$$\frac{J_\infty-J}{1-J}=\frac{J_\infty-(1-k)}{k}e^{-E}, \tag{C9}$$

$$E(\Delta)=\frac{1-J_\infty}{J_\infty-(1-k)}f_m(\Delta-\Delta_s) \tag{C10}$$

and consequently

$$J(\Delta)=1+\frac{J_\infty-1}{1-\frac{(1-k)\kappa}{k}e^{-E(\Delta)}} \tag{C11}$$

Using the identities $2(1+e^{-2Y})^{-1}=1+\tanh Y$ and $2(1-e^{-2Y})^{-1}=1+\coth Y$ we combine the results **Eqs C6** and **C11** to the analytical approximation of the SIR-model equations at all reduced times, stated in **Eqs 10–12** above. A comparison with the exact numerical solution of the SIR model is provided in **Figure C2**. The corresponding $j(\Delta)$ is obtained from $J(\Delta)$ via **Eqs A5**.

APPENDIX D: SI-LIMIT $k = 0$

In the limit $k = 0$ **Eq. A7** provides $J_0(k=0)=1/2$ so that with $\lim_{k\to 0} f_m(k=0)=1$ the time scale (**Eq. C3**) becomes

$$\Delta_s(k=0)=\lim_{k\to 0}\ln\frac{1-k}{k}=\infty \tag{D1}$$

With this result

$$Y_1(k=0)=\frac{\Delta}{2}-\frac{1}{2}\lim_{k\to 0}\left[\Delta_s+\ln\frac{k}{1-k}\right]$$
$$=\frac{\Delta}{2}-\frac{1}{2}\lim_{k\to 0}\left[\ln\frac{1-k}{k}+\ln\frac{k}{1-k}\right]=\frac{\Delta}{2} \tag{D2}$$

Consequently, the cumulative number **Eq. 10** and the rate **Eq. 4** in this case for all times correctly reduce to

$$J(\Delta,k=0)=\frac{1}{2}\left[1+\tanh\frac{\Delta}{2}\right],\qquad j(\Delta,k=0)=\frac{1}{4\cosh^2(\Delta/2)} \tag{D3}$$

APPENDIX E: RELATIONSHIP BETWEEN J_0 AND K

Here we prove **Eq. 14**. According to paper A the quantity J_0 is given by $J_0=1-e^{-G_0}$ with

$$G_0=\frac{1+k}{k}+W_{-1}\left(\frac{-2e^{-1/k}}{ke}\right)=-\ln(1-J_0) \tag{E1}$$

where e denotes Euler's number and W_{-1} the non-principal solution of Lambert's equation $z=We^W$. **Equation E1** is of the form $x=r+c^{-1}W(ce^{-cr}/\beta)$ upon identifying $c=1$, $r=1/k$, $\beta=-ke/2$, and $x=-[1+\ln(1-J_0)]$. From paper A we thus know that $e^{-cx}=\beta(x-r)$ holds, or equivalently

$$(1-J_0)e=-\frac{ke}{2}\left[-1-\ln(1-J_0)-\frac{1}{k}\right]=\frac{ke}{2}[1+\ln(1-J_0)]+\frac{e}{2} \tag{E2}$$

This is readily solved for k, and thus proves **Eq. 14**.

APPENDIX F: TIME OF MAXIMUM IN THE MEASURED DIFFERENTIAL RATE $\dot{J}(t)$

One has $J(t)=J(\tau(t))$ and $\dot{J}(t)=\dot{\tau}(t)J'(\tau(t))=a(t)j(\tau(t))$ since $j=J'$ if we let the prime denote a derivative with respect to τ. The maximum in $\dot{J}(t)$ thus fulfills

$$0=\ddot{J}(t_m)=\dot{a}(t_m)j(\tau(t_m))+a^2(t_m)j'(\tau(t_m)) \tag{E1}$$

or equivalently,

$$0=\left[\frac{d\ln j}{d\tau}+\frac{\dot{a}}{a^2}\right]_{t=t_m} \tag{E2}$$

From part A we know that

$$\frac{d\ln j}{d\tau}=1-2J-k\ln(1-J)-k \tag{E3}$$

and our $J_0=J(\tau_0)$ solves $1=2J_0+k\ln(1-J_0)+k$. That is, $j'(\tau_0)=0$. If a does not depend on time, $\tau_0=\tau(t_m)=a_0t_m$, but this is not generally the case. To find t_m and $\tau_m\equiv\tau(t_m)$ one has to solve **Eq. E1**, or **Eq. E2**. **Equation E2** with **Eq. E3** is solved by

$$J_m=J(\tau_m)=1+\frac{k}{2}W_{-1}(\alpha_m) \tag{E4}$$

with

$$\alpha_m=-\frac{2e^{-(1+C_m)/k}}{ek},\quad C_m=-\frac{\dot{a}(t_m)}{a^2(t_m)} \tag{E5}$$

The corresponding j is, according to **Eq. 4**,

$$j(\tau_m)=(1-J_m)[J_m+k\ln(1-J_m)] \tag{E6}$$

The smaller C_m, the closer is J_m to J_0.

APPENDIX G: FITTING THE DATA

As discussed in length in paper A we base our analysis of existing data on the reported cumulative number of deaths, $D(t)$, from which we estimate the cumulative number of infections $J(t)=D(t-t_d)/f=200D(t-t_d)$ with $t_d=7$ days. From the cumulative value $J_m=J(t_m)$ at the time t_m of the maximum in $\dot{J}(t)$ we estimate k via **Eq. 14** upon assuming $J_m\approx J_0$. Similarly, $a_m=a(t_m)$ is estimated from $a_m=\dot{J}(t_m)/j_{\max}(k)$. These t_m, k, a_m are not the final values, but provide starting values which are then used in the minimization of the deviation between measured and modeled $J(t)$. The minimization is performed assuming the time-dependent $a(t)$ parameterized by **Eq. H1** involving parameters $t_a>0$, $t_b>0$, $a_0>0$, $q\in[0,1]$, $q<\eta\in[0,1]$ and $t_s>t_m$. While $\tau(t)$ is given by the integrated $a(t)$, we use three strategies to model $J(t)$: i) the numerical solution of the SIR model, ii) the

approximant $G(\tau)$ and $J(\tau) = 1 - e^{-G(\tau)}$ developed in part A, and iii) the approximant $J(\Delta)$ given by **Eq. 10** with $\Delta = \tau - \tau_m$ and τ_m specified by **Eq. 9**. Because the numerical solution (i) is extremely well approximated by (ii), and (ii) and (iii) compared to (i) not prone to numerical instabilities at small and large Δ, we present results only for method (iii), as they can be readily reproduced by a reader without Lambert's function at hand.

APPENDIX H: MODELING OF LOCKDOWN LIFTING

Similarly to the lockdown modeling a later lifting of the NPIs can be modeled by adopting the infection rate

$$a(t) = a_{\rm LD}(t)\,\Theta(t_s - t) + a_{\rm stop}(t)\,\Theta(t - t_s) \tag{H1}$$

where t_s denotes the stop time of the lockdown still represented by the infection rate **Eq. 15**, and where $a_{\rm LD}$ is given by **Eq. 15**. The infection rate after t_s is assumed to be

$$a_{\rm stop}(t) = a_0\left[q_s + (\eta - q_s)\tanh\frac{t - t_s}{t_b}\right] \simeq \begin{cases} q_s a_0 & \text{for } t = t_s \\ \eta a_0 & \text{for } t \gg t_s, \end{cases} \tag{H2}$$

with $q_s = a_{\rm LD}(t_s)/a_0$ the quarantine factor reached at the time t_s of lifting. Together with the reduced time given by **Eq. 16** we now find

$$\tau(t) = \tau_{\rm LD}(t)\,\Theta(t_s - t) + \tau_{\rm stop}(t)\,\Theta(t - t_s) \tag{H3}$$

and

$$\tau_{\rm stop}(t) = \tau_{\rm LD}(t_s) + q_s(t - t_s)a_0 + (\eta - q_s)a_0 t_b \ln\left[\cosh\left(\frac{t - t_s}{t_b}\right)\right] \tag{H4}$$

with $\tau_{\rm LD}(t)$ from **Eq. 16**. For the four basic types of **Figure 4** we demonstrate in **Figure 7** the effect of incomplete lifting.